53rd AIAA/ASME/ASCE/AHS/ASC Structures, Structural Dynamics and Materials Conference
20th AI
23 - 26 April 2012, Honolulu, Hawaii

AIAA 2012-1949

Homogenization of slender periodic composite structures

Julian Dizy[1], Rafael Palacios[2], and Silvestre T. Pinho[3]
Imperial College, London, SW7 2AZ, United Kingdom

A homogenization technique is developed to obtain the equivalent 1-D stiffness properties of complex slender periodic composite structures with varying cross-sections. All this is done while removing the limitation of a constant cross-section often imposed in literature. The problem is posed using a unit cell approach and applying periodic boundary conditions such that: 1) the microscopic strain state averages to the macroscopic conditions, and 2) the deformation energy is conserved between scales. The methodology also allow for stress recovery and local buckling analysis. Numerical examples are shown to illustrate the diverse capabilities of the method: an isotropic ribbed prismatic beam is used to introduce the method, show the reinforcements and local buckling capabilities; a composite laminated cylinder is shown to demonstrate span-wise varying properties and parametric analysis and, finally, a composite blade section exemplifies it for complex geometries.

Nomenclature

b	=	unit cell depth
$\mathcal{C}_{ijkl}$	=	material elasticity tensor
θ_i	=	macroscopic local rotations
E	=	Young's modulus
ϵ	=	beam strains
ε_{ij}	=	Cauchy's strain tensor
G	=	shear modulus
ν	=	Poisson's ratio
L	=	length of the beam
Ω	=	volume of the unit cell
$\mathcal{S}_{4\times4}$	=	homogenized stiffness matrix
$\mathcal{U}$	=	elastic strain energy
u_i	=	macroscopic local displacements
v_i	=	microscopic displacement field
w_i	=	warping field

I. Introduction

DESPITE huge advances in computational power in the last decade, which allow direct solid modeling of most aerospace structures, there is still a practical interest in dimensionally-reduced structural models. Beam models, in particular, can provide excellent approximations of the primary structures for low-frequency aeroelastic analysis of high-aspect-ratio wings, helicopter rotor blades or wind turbines. The simplicity of construction of the models also makes them essential tools in many other applications for conceptual studies. A great deal of effort has been put into developing composite beam models [1], able to account for elastic couplings in reduced one-dimensional models. In general, the modeling process can be split into two different stages: Firstly, there is a *homogenization step,* which determines the constitutive relations of the reduced model (i.e., sectional properties of the beams); secondly, there is a *solution step*, in which one evaluates the response of the dimensionally-reduced model to the set of applied loads. Both stages are interrelated as assumptions on one affect the other. The equations of motion in the *solution stage* have been well developed, including geometrically-nonlinear effects, in the works of, for instance,

[1] Graduate Student, Department of Aeronautics, AIAA Student Member.
[2] Lecturer, Department of Aeronautics, (Contact author. e-mail: rpalacio@imperial.ac.uk), AIAA Member.
[3] Senior lecturer, Department of Aeronautics.

Copyright © 2012 by Julian Dizy, Rafael Palacios and Silvestre T. Pinho. Published by the American Institute of Aeronautics and Astronautics, Inc., with permission.

Simo and Vu-Quoc [2]; Cardona and Geradin [3] and Hodges [4, 5]. The constitutive relations in the first stage have been mostly obtained under the assumption of constant (or slowly-varying) cross sections. In our case, only the homogenized section metrics need to be slow varying. The constitutive relations are the focus of this work.

For composite beams, one of the most successful approaches in dealing with arbitrary sectional properties is the Variational Asymptotic Method (VAM) [6]. The cross-sectional analysis calculates the 3-D warping functions asymptotically and finds the constitutive model for the 1-D nonlinear beam analysis. After the global deformation from the 1-D beam analysis is obtained, the original 3-D displacements, stresses and strains can also be recovered using the already available 3-D warping functions. It is worth noting that solutions based on VAM only work well away from the beam boundaries or sudden changes in the cross-sectional geometry along the span (including transverse reinforcements). Very recently, Lee and Yu [7] have proposed, as a remedy to that shortcoming, to use the smallness of the heterogeneity and incorporate a dimensional reduction, simultaneous to the homogenization step, to the variational asymptotic method. Another possibility is to use the Formal Asymptotic Method [8-10]. It exploits the existence of two scales in the original dynamic 3D equations governing the beam structure to perform an asymptotic homogenization. However it has a few disadvantages such as finding an adequate set of boundary conditions, implementing it numerically or adapting it to simple engineering models [7]. A further possibility is that proposed by Kennedy and Martins [11] which builds the kinematic description of the beam based on a linear combination of fundamental state solutions, which are axially-constant, and calculated at the mid plane of the beam by using a 2D finite-element method to obtain the stresses and strains due to the Saint-Venant (axial, bending, torsion and shear) [12] and Almansi-Michell (distributed surface load) loadings [13]. This method yields FEM comparable accurate solutions as long as the sections do not vary along the axis of the beam and the loads are statically determined.

The previous solutions either were limited to constant-section geometries, or required dedicated –and often quite involved– implementations. Furthermore, they are linear approaches that do not provide information about the strength of the structure. Due to their high strength-stiffness ratio, composite thin wall structures usually exhibit local or distortional buckling before material failure [14] and this is often a design constraint. The objective of the present work is to introduce a general methodology to evaluate both the elastic constants and the local buckling strain of composite beams, with periodic properties along the spanwise direction, which can be implemented into a general-purpose finite-element code. The method is based on the analysis of a unit cell, which defines a local scale much smaller than the characteristic wavelength in the beam response. This is formally similar to the work of Lee and Yu [7] but the final equations to obtain the beam stiffness constants can be solved using periodic boundary conditions in most off-the-shelf finite-element solvers. Application of this approach to high-aspect ratio vehicle analysis is expected to improve the accuracy of the results in the conceptual stage of design, reducing the time and cost of the whole design process and bringing project inception and flight readiness closer together.

II. Theory

Consider a slender prismatic solid made by repeating a periodic cell along its longitudinal dimension $-\frac{L}{2} \leq y \leq \frac{L}{2}$ (see Figure 1). The transverse dimensions of the structure, h are much smaller than the characteristic longitudinal dimension $h \ll L$. The coordinate y in the reference configuration defines the reference line for the 1-D macroscopic (beam) which coincides with the neutral axis. The longitudinal dimension of the cell is $b \ll L$. We are interested in the linear homogenized elastic constants, so linear assumptions will be also used for the kinematics and the local material properties.

The adopted solution relies on two assumptions made between scales to deduce a set of periodic boundary conditions and obtain the beam stiffness constants [15]. These assumptions are: a) the large scale variables are an average of the small scale ones, and b) the deformation energy is conserved between scales. The formulation described here is, at this stage, a first-order theory and does not include the effects from transverse shear which are still being investigated. All throughout this section, Einstein notation is used for repeated indices, with Latin indices

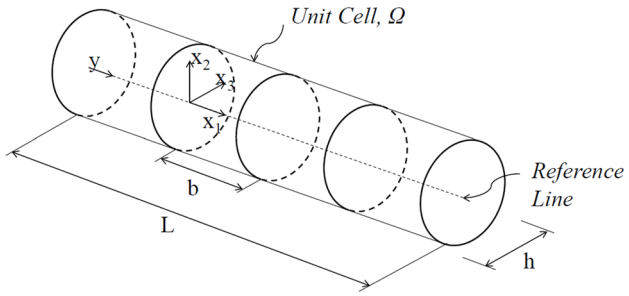

Figure 1: Schematic diagram of the continuum beam with the unit cell representation.

assuming values from 1 to 3 and Greek ones assuming values of 2 and 3.

A. Kinematics

Under linear assumptions, the deformation of the reference line can be described by three local displacements $u_i(y)$ and three local rotations $\theta_i(y)$ with respect to the x_i coordinate system in Figure 1. The beam strain measures are obtained from linearization of the strain-displacement kinematic relations in Ref. [16], as

$$\gamma_1(y) = u_1'; \; \gamma_\alpha(y) = u_\alpha' - e_{\alpha\beta}\theta_\beta; \; \kappa_i(y) = \theta_i' \tag{1}$$

with $e_{\alpha\beta}$ being the Levi-Civita or permutation symbol. If we further assume $\gamma_\alpha(y) = 0$, i.e., a first-order theory, that implies

$$\theta_2 = -u_3'; \; \theta_3 = u_2' \tag{2}$$

We define the vector of first-order beam strains containing extensional strain γ_1, bending curvatures in two directions κ_2, κ_3 and torsional curvature κ_1, as

$$\epsilon^{\mathrm{T}} = \{\gamma_1 \quad \kappa_1 \quad \kappa_2 \quad \kappa_3\} \tag{3}$$

At the small scale level, we consider the 3-D deformation of a cell of volume Ω centered at *y* (see Figure 1). The undeformed position within the cell will be given by coordinates x_i, where x_1 is parallel to y, but measures lengths at cell scales (i.e., $\frac{dx_1}{dy} = \frac{b}{L}$), so it can be seen as magnified coordinate system. The three components of the microscopic displacement field are $v_i(y; x_1, x_2, x_3)$. The two longitudinal dependencies are introduced to separate between *small scale*- ($\sim x_1$) and *large scale*-fluctuations ($\sim y$) of the structural deformations [7]. The microscopic and macroscopic variables can be related through an arbitrary *warping field*, as

$$\begin{aligned} v_1(y; x_1, x_2, x_3) &= u_1(y) - e_{\alpha\beta}x_\alpha\theta_\beta(y) + w_1(y; x_1, x_2, x_3), \\ v_\alpha(y; x_1, x_2, x_3) &= u_\alpha(y) - e_{\alpha\beta}x_\beta\theta_1(y) + w_\alpha(y; x_1, x_2, x_3), \end{aligned} \tag{4}$$

Note that if the warping field is zero, Eq. 4 is the kinematic assumption used in Timoshenko beam theory (or Euler-Bernoulli theory if the condition of Eq. 2 is enforced, which has been referred to as the *fundamental solution* in asymptotic theories [10]. In general the warping field will depend on the cell and it was explicitly written as a function of y.

The independent macroscopic variables will be defined from averages in the cell, as

$$u_i(y) = \langle v_i \rangle; \; \theta_1(y) = \frac{1}{2}\langle v_{3,2} - v_{2,3} \rangle \tag{5}$$

where $\langle \bullet \rangle = \frac{1}{\Omega}\int_\Omega \bullet \, dx_1 dx_2 dx_3$ and $\bullet_{,j} = \frac{\partial \bullet}{\partial x_j}$. If we take the reference axis at the centroid, i.e. $\langle x_\alpha \rangle = 0$, then these definitions impose four constraints on the warping field,

$$\langle w_i \rangle = 0; \; \langle w_{2,3} - w_{3,2} \rangle = 0 \tag{6}$$

B. Equilibrium conditions

Our interest is in the interior solution of the problem to obtain the homogenized stiffness constants, $\mathcal{S}_{4\times4}$, and these can be obtained simply by assuming constant large scale strains, that is, $\epsilon(y) = \bar{\epsilon}$. We then postulate constitutive relations in the homogenized problem such that strain energy is conserved between the small and large scale levels [15]. Due to the periodicity of the problem, the microscopic strain energy will be independent of the cell in the interior solution and it will be

$$\mathcal{U} = \frac{b}{2}\bar{\epsilon}^T \mathcal{S}\bar{\epsilon} = \int_\Omega \mathcal{C}_{ijkl}\varepsilon_{ij}\varepsilon_{kl}dx_1dx_2dx_3, \tag{7}$$

with $\mathcal{C}_{ijkl}(x_1, x_2, x_3)$ being the material elasticity tensor and $\varepsilon_{ij} = \frac{1}{2}(v_{i,j} + v_{j,i})$ the components of the local strain tensor. Define now the magnitudes $\Delta v_i = v_i\left(y; \frac{b}{2}, x_2, x_3\right) - v_i\left(y; -\frac{b}{2}, x_2, x_3\right)$. Eq. 4 becomes

$$\begin{aligned} \Delta v_1(y; x_2, x_3) &= \bar{\gamma}_1 b - e_{\alpha\beta}x_\alpha \bar{\kappa}_\beta b + \Delta w_1(y; x_2, x_3) \\ \Delta v_\alpha(y; x_2, x_3) &= -e_{\alpha\beta}x_\beta \bar{\kappa}_1 b + \Delta w_\alpha(y; x_2, x_3). \end{aligned} \tag{8}$$

For this solution to be independent of the cell, it must be $\Delta w_i(y; x_2, x_3) = 0$, i.e., the warping field is periodic. This can also be concluded arguing that, due to periodicity, the strain field must be compatible and the only difference in displacement allowed between both faces of the cell is a rigid body motion, which does not create strain. We are finally left with the problem of obtaining the static equilibrium conditions on a generic cell under an applied displacement field given by

$$\begin{aligned} v_1(\frac{b}{2}, x_2, x_3) &= v_1(-\frac{b}{2}, x_2, x_3) + \bar{\gamma}_1 b - e_{\alpha\beta}x_\alpha \bar{\kappa}_\beta b, \\ v_\alpha(\frac{b}{2}, x_2, x_3) &= v_\alpha(-\frac{b}{2}, x_2, x_3) - e_{\alpha\beta}x_\beta \bar{\kappa}_1 b \end{aligned} \tag{9}$$

This problem can be set up on any standard finite element package using multipoint constraints to enforce periodic boundary conditions.

III. Numerical implementation

There are three basic steps in the implementation of the homogenization procedure described above which have been schematized in Figure 2:

I. The geometry of the cell is created using a Python script whose inputs are dimensions, mesh density and material properties. Using this data an Abaqus standard input file is generated including a set of periodic boundary conditions from Eq. (9). Each loading case is introduced via a different *master node* for which prescribed displacements are applied.

II. The model is meshed using 'C3D8R' (3D-cuboid-8node) elements with reduced integration for the calculation of the stiffness properties and 'C3D8'in case of a buckling analysis. This is due to the complexity of buckling deformed shapes and hence the likelihood of hourglassing and other convergence problems. For the anisotropic cases, each element has its own local coordinate system which coincides with the axis of the element and each composite ply is modeled with a layer of elements.

III. A set of analysis is then performed: a standard linear elastic with ten steps –corresponding to each of the loadings and the pair-wise combinations of these–, and a linear perturbation analysis for the axial case.

IV. Then the binary output database (.odb) file generated from the analysis is read automatically. This step further justifies the use of Python as Abaqus uses this language internally for analysis and database organization. Finally, the elastic strain energy is integrated for the whole model and using Eq. (7) the stiffness terms are calculated and printed to an output text file.

Note that this approach is however independent of our particular implementation here. The input file is a standard Abaqus model and requires no user-defined modules in the FE solver.

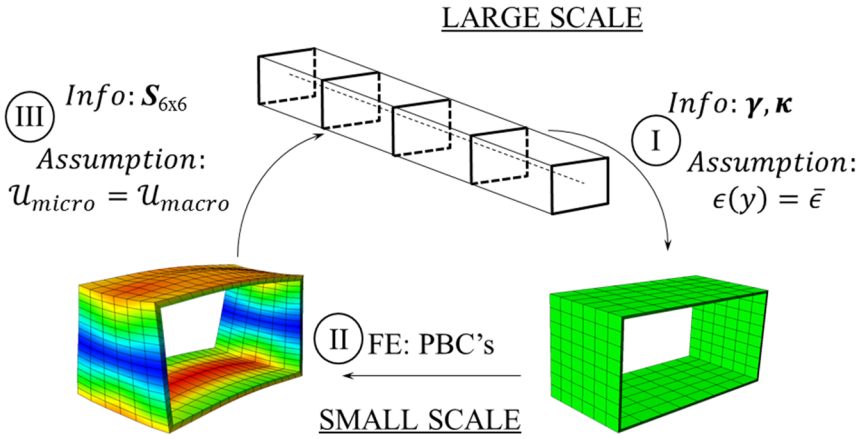

Figure 2: Flow of information between the large and small scales

IV. Numerical studies

The methodology described above is exemplified here via three models subject to five case studies of increasing complexity. Each of them presents a unique feature of the methodology. The first case is a model of a prismatic isotropic beam for which analytical results exist. The study is complemented with two extra subcases of transverse shear effects and transverse reinforcements. The second and third cases are based on a laminated thin walled cylinder used to substantiate the implementation of composite materials and compare the results to those obtained using UM/VABS [17]. In the third case 3D capabilities of the method are showcased by comparing a prismatic cell with varying cross-sectional thickness to a full model consisting of 20 cells under static loads and performing a parametric analysis on an *y*-axis dependent variable. The forth case refers to the introduction of the local buckling strain prediction. Finally the fifth case is a highly complex rotor blade section which encompasses many of the key points of this theory: material orientations, reinforcements and asymmetric geometry.

A. Isotropic prismatic beam with transverse reinforcements

The model is a ribbed prismatic box beam made out of homogenous isotropic material (aluminum: E=70GPa, ν=0.3) with dimensions of *width*=2m, *height*=1m and a total thickness of 0.025m along all walls. The distance between ribs is b=1m which results in 1m unit cells and a full beam model of L=20m. The full beam is built-in on one end and all the loads or moments are applied via a rigid body node-constraint and a reference point at the other end. The geometry is shown in Figure 3.

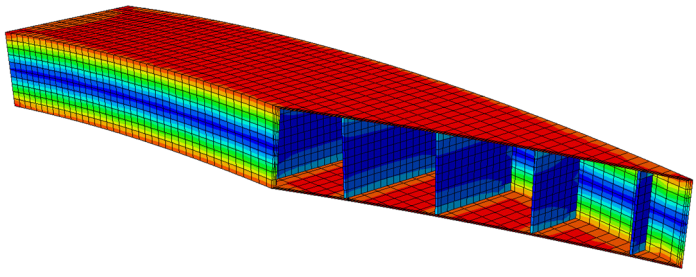

Figure 3: Vertical cut of the full beam FE model with reinforcements illustrating the mesh.

The results are summarized in Table 1 and compared with results without ribs obtained by: a) analytical results from thin-walled beam theory; b) full beam analysis using Abaqus and static loading; c) UM/VABS. The last column shows the effect of adding a transverse wall of the same thickness of the outer walls at the mid-span position of every cell.

The agreement of the results produced by this homogenization method is excellent both with the theory and the current available tools. The small discrepancy that thin-wall theory has, in the case of torsion, with both UM/VABS

and the proposed method, is due to the thin-wall assumption of the former and it is the latter techniques which are more accurate. The addition of the transverse wall resulted in very little improvement in stiffnesses as it was expected from a thin flat plate positioned at right angle with respect to the beam axis. The von-Mises stress contour of the full beam with reinforcements for a bending moment load can also be seen in Figure 3.

Table 1: Stiffness constants for the prismatic box beam obtained from different methods.

Stiffness constant	No ribs				With ribs
	Analytical (Thin wall)	FE (full beam)	UM/VABS	Present method	Present method
$S_{11}(EA)$ [GN]	10.3	10.3	10.3	10.3	10.5
$S_{22}(GJ)$ [GNm²]	1.79	1.71	1.71	1.71	1.72
$S_{33}(EI_{zz})$ [GNm²]	1.91	1.91	1.91	1.91	1.94
$S_{44}(EI_{yy})$ [GNm²]	5.58	5.58	5.58	5.58	5.62

B. Laminated cylinder with constant ply angle and span-wise variable thickness

In this example, there are two subcases: a 2-ply, constant fiber orientation angle circular cylinder used to demonstrate the stiffness variation as the ply angle changes and then a modified section of this used to exemplify the parametric capabilities of the method dealing with varying thickness cross sections. Material orientations are taken clockwise around the normal vector of the element with the x_1 direction as the reference for a zero degree ply angle.

Table 2: Material properties of the composite used in the laminated cylinder

E_{11}=1.42×10¹¹ Pa	E_{22}= E_{33}=9.8×10⁹ Pa
G_{12}=G_{13}=6.0×10⁹ Pa	G_{23}=4.8×10⁹ Pa
ν_{12}= ν_{13}=0.3	ν_{23}=0.3

The dimensions of the constant sections are unitary radius, R=1m measured to the outer wall, and 5% thickness, t=0.05m as depicted in Figure 4. The length of the unit-cell model, which does not affect the homogenized results, is b=0.1m. The material properties of the composite used are given in Table 2.

The non-zero terms of the 4x4 stiffness matrix have been plotted in Figure 5 together with the results obtained using UM/VABS [17]. These terms include: extensional (S_{11}), torsional (S_{22}), and bending (S_{33}) stiffnesses plus the coupling between the first two (S_{12}). (Only one bending stiffness is shown as the section is symmetric.) The evolution of these constants with the ply angle agrees very well between both methods and the error is always less than 0.1%.

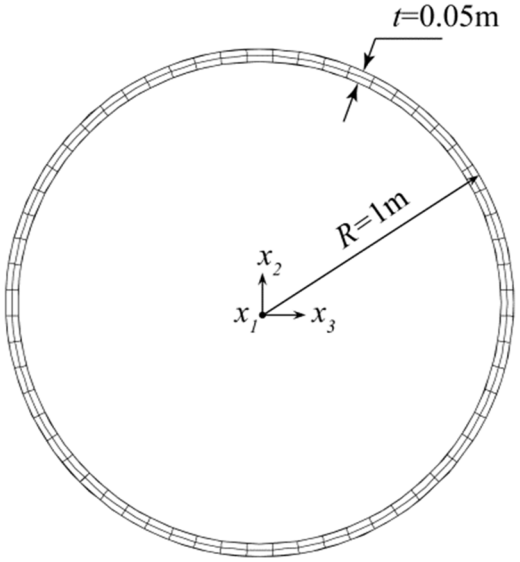

Figure 4: Cross-sectional discretization of the circular section and its dimensions. (Cell model is 3-D.)

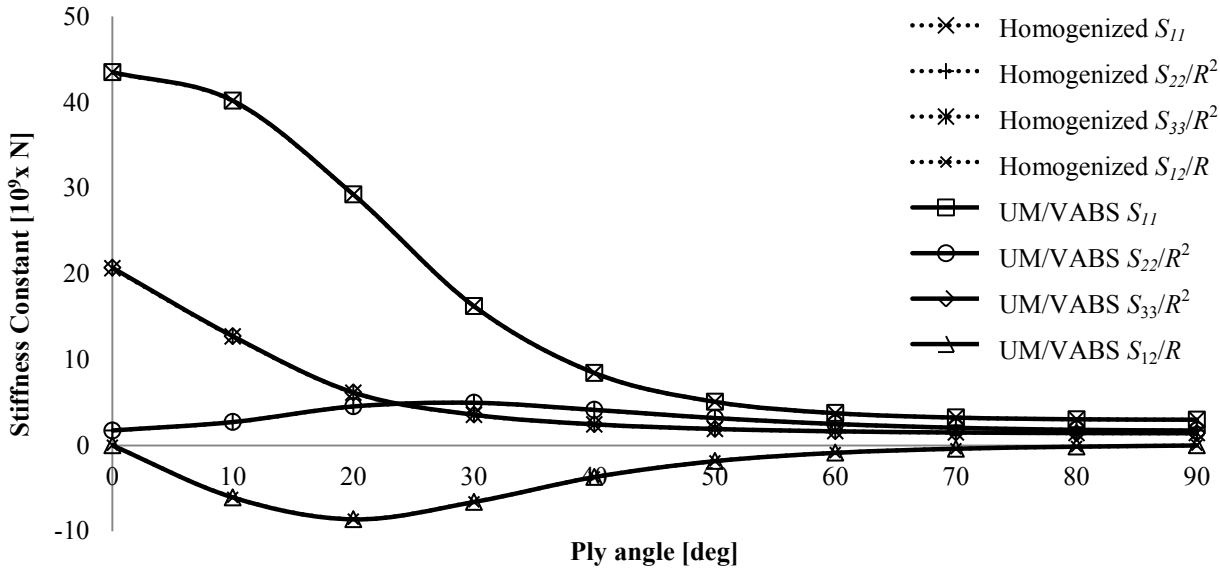

Figure 5: Stiffness constants as a function of the ply angle for the cylinder with constant cross sections.

A modified version of the previous example will be used next to explore the capabilities of the method to model 3D cells that include heterogeneity along the x_1 direction. For that purpose, the outer radius will remain the same but the thickness of the section will vary as a function of the span wise position. This change consists of a 25% reduction in thickness of the inner sections ('*a*' region) with a linear variation region joining the outermost sections which remain the same thickness. The material properties are those from Table 2. This is depicted in Figure 6.

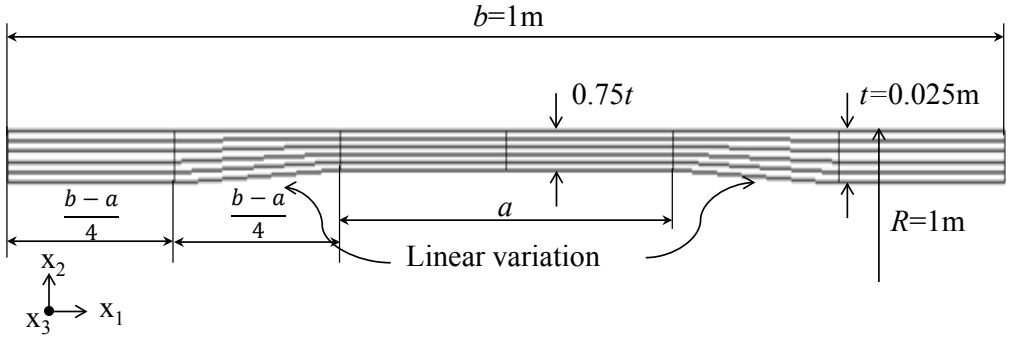

Figure 6: Longitudinal cut of the cell showing the thickness variation

The composite layup is now a $[45,-45,0,90]_s$. In order to assess the performance of the methodology, the results will be compared to a full size FE analysis in Abaqus of a 10-cell beam created with a tessellation of the cell just described clamped on one end and with a κ_1=0.1 equivalent moment applied. It is worth noting that the unit cell model runs almost instantaneously but the full-size model requires over *8GB RAM* and takes two orders of magnitude longer to run. Figure 7 shows how the top nodes (x_2=*R*, x_3=0) deflect as a function of x_1 in the full model as compared to the deflection of a beam of the homogenized stiffness under the same load. Both solutions are very close with minor discrepancies at the boundaries of the beam, since *end effects* are not accounted for in the homogenized model. Table 3 contains the von Mises stress values through the thickness of all the plies at a 45º angle cut (x_2=x_3=$\sqrt{2}$/2m) at the mid-span location (x_1=*b*/2m). It corroborates that the technique not only predicts homogenized stiffness and displacements correctly, but it also provides stress levels across the plies.

Table 3: Interpolated von Mises stress values across plies at mid-span nodes.

Ply angle [deg]	von Mises stress [MPa]	
	Homogenized	FE (full beam)
45	400.0	400.5
-45	386.0	386.5
0	910.1	910.3
90	211.2	210.9
90	209.1	208.8
0	780.2	780.9
-45	283.7	278.9
45	233.4	239.0

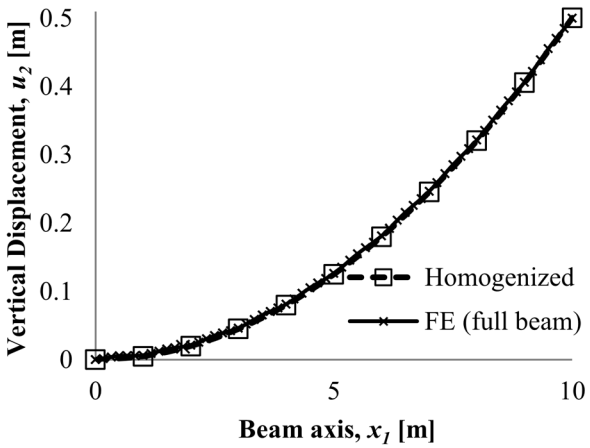

Figure 7: Vertical deflection of the top nodes

Given the level of automation of the mesh generation it is easy to perform a parametric analysis to check the sensitivity of the structure to variations of one (or more) of its variables. In this case, the effect of the thickness of the wall has been studied. This is done by increasing the relative length of the '*a*' region (25%-reduced thickness part) with respect to the total length, *b*. The results are plotted in Figure 8 . Note that in the limit when a/*b*=1 this corresponds to a cylinder of constant thickness 0.75*t*. The evolution of the stiffness parameters follows an expected mild decrease as the thickness is reduced.

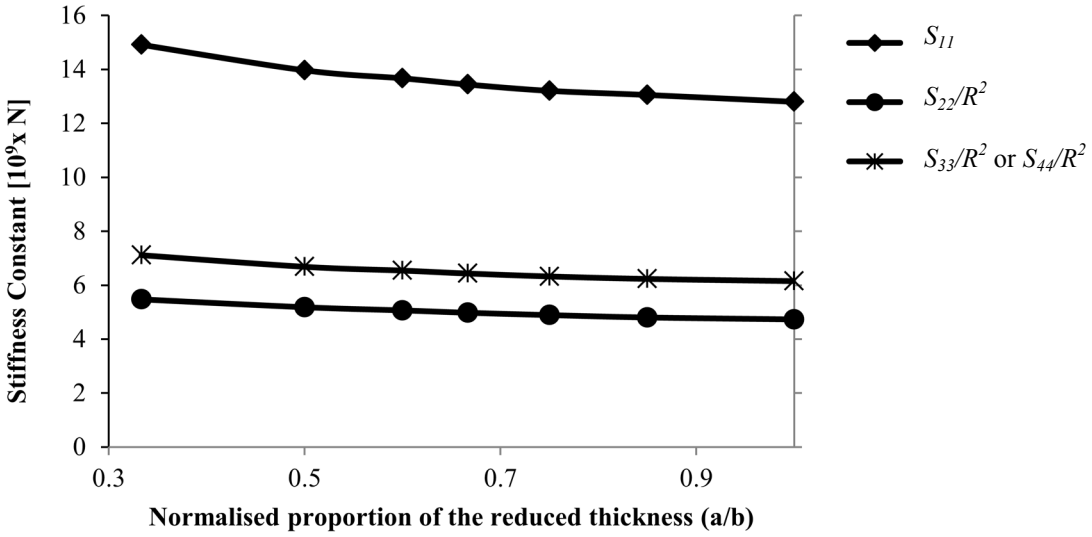

Figure 8: Parametric analysis on the thickness effect for a laminated cylinder

C. Local buckling of a reinforced prismatic beam

This case explores the suitability of a unit cell analysis to obtain local buckling loads under compressive loads. Global buckling is not accounted for here but instead computed by the beam model. The model used is similar, in shape, to that of case A -a prismatic beam with perpendicular wall reinforcements- but the thickness of the skin and the reinforcement have been modified to exhibit a characteristic skin-buckling response. The new dimensions are hence: 1mm for the skin and 10cm for the reinforcement. All other model properties are kept the same as in the aforementioned case. As it can be seen from Figure 9 the deformed shape of the structure is coincident in both models -the unit cell and the full 3D one-. Note the deformation scales are the same so they can be readily compared

graphically. It is clear that both approaches find the same solution for the first buckling failure mode. Furthermore, the magnitude of the loading at which this would occur (eigenvalue) is found to be very close: $\gamma_{1,buckling}$=0.030427 for the full 3D model and $\gamma_{1,buckling}$=0.030583 times for the unit cell.

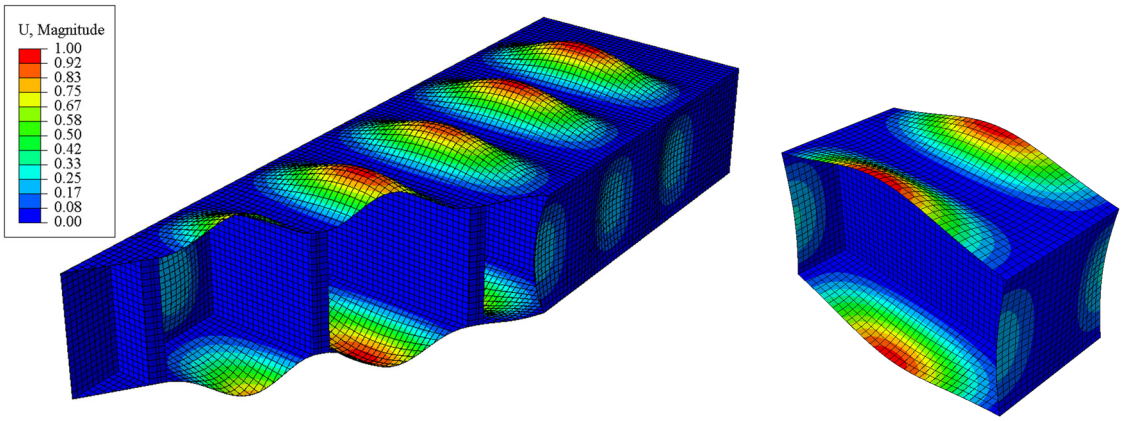

Figure 9: Contour plot of the first eigenshape of a ribbed prismatic beam under compressive loads. Full beam shown on the left and unit cell on the right.

D. Active Twist Rotor blade

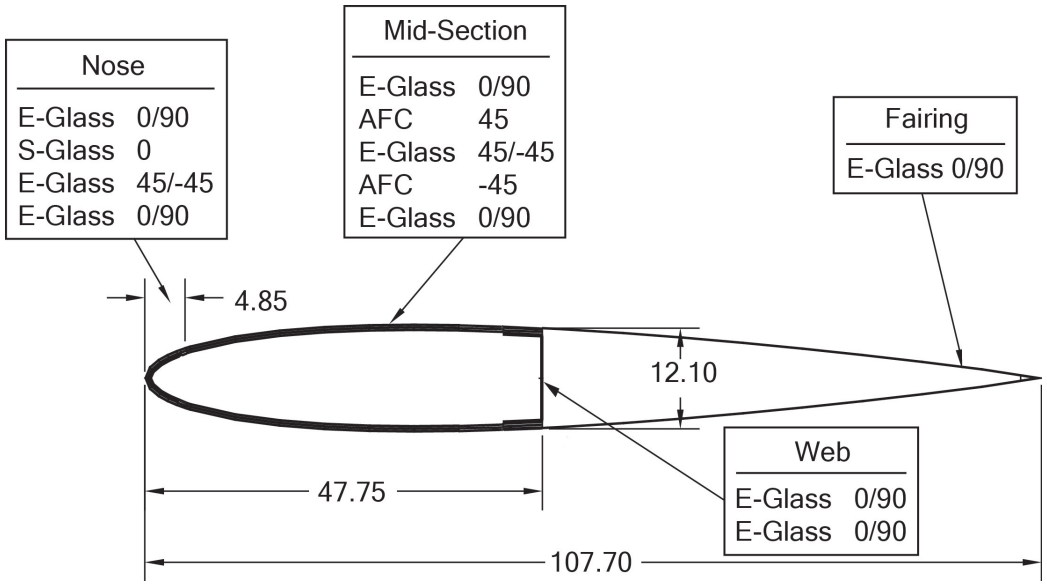

Figure 10: Dimensions (in mm) of the ATR blade with the composite layups

The ATR blade from NASA and MIT brings a higher level of complexity (both in the material and geometrical definitions) which allows further verification of the approach. The dimensions of the cross section are depicted in Figure 10 and its material properties described in Table 4. More details can be found in Cesnik & Ortega [18]. The cross section has been modelled without the foam core that it sometimes contains, and extruded to a total depth of 20% the maximum cross sectional dimension (the default by the mesher). It is worth noting, that unlike other solutions, the current method allows for more than one part to be present in the assembly of the structure and the corresponding meshes can be joint together by specifying tie-constraints. Even though this may seem more complicated at first than just having a single part, it multiplies the scalability and possibilities of the reinforcements added and what is more important, it sets the basis for a future material bond integrity research (delamination, etc.). The results, shown in Table 5 are in full agreement with the existing techniques and the discrepancies never exceed ~5% .

Table 4: Material properties of the ATR wing [18]

Material Property	Units	E-Glass (Style 120 Fabric)	S-Glass (Unitape)	AFC
E_L	GPa	20.7	46.9	22.18
E_T	GPa	20.7	12.1	14.91
G_{LT}	GPa	4.1	3.6	5.13
ν_{LT}	-	0.13	0.28	0.454
t_{PLY}	mm	0.114	0.229	0.203

Table 5: Stiffness constants comparison between different methods

Stiffness constant *(% diff w.r.t. present method)*	VABS-A		UM/VABS		Present method
S_{11} [N]	1.684	*(0.4%)*	1.677	*(0.0%)*	1.677
S_{22} [Nm²]	34.70	*(-0.1%)*	34.79	*(0.1%)*	34.75
S_{33} [Nm²]	41.64	*(0.8%)*	41.18	*(-0.2%)*	41.29
S_{44} [Nm²]	1031.	*(-3.5%)*	1086.	*(1.5%)*	1069
S_{12} [Nm]	-13.07	*(3.1%)*	-12.72	*(5.7%)*	-13.49
S_{14} [Nm]	250.7	*(0.8%)*	243.4	*(-3.7%)*	252.8

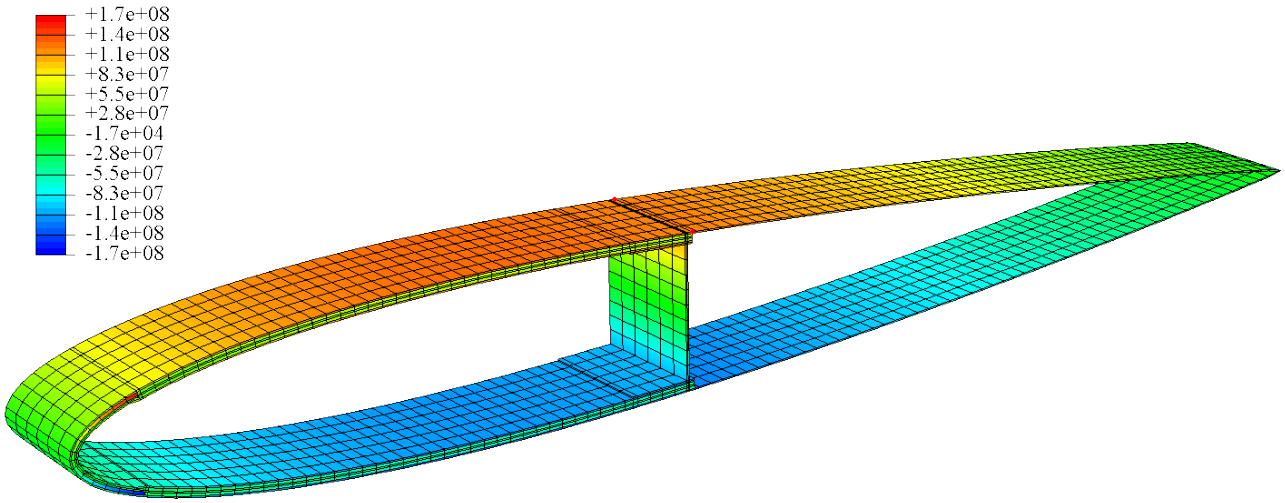

Figure 11: stress recovery example for the direct x_1-component of stress on an ATR wing for $\kappa_1 = 0.1$. Units in Pa.

V. Conclusion

A new approach to obtaining homogenized properties of slender periodic composite structures has been presented. The methodology is based on the equivalence between the strain states at the macro- and micro-scales and the conservation of strain energy between both. The implementation via periodic boundary conditions and a standard FEA package has also been described. The use of a 3D unit cell eliminates all previous constraints of constant cross-sections and non-varying properties along the length (span) of the beam; and leads to a more sophisticated analysis on slender structures at a preliminary stage at a very low computational cost. The modeling of the geometry is fully parametric which allows sensitivity analysis to be done. The way the loadings are introduced into the model and the final outputs exported make this approach readily compatible with aeroelastic optimization based on "stick models" [19]. The numerical examples show a down-to-discretization agreement with other available methods and, to the knowledge of the authors, demonstrate local buckling strain calculated in a beam's unit cell for the first time in literature. In the future, the interfaces between the different parts of a model will be further exploited to introduce material integrity calculations with relative simplicity. Overall, this method is a very flexible and powerful candidate to obtain the homogenized stiffness and local buckling loads of an arbitrarily-shaped periodic (or constant-section) composite beam.

References

1. Hodges, D., *Nonlinear Composite Beam Theory*. Progress in Aeronautics and Astronautics. Vol. 213. 2005, Reston, VA: AIAA.
2. Simo, J. and L. Vu-Quoc, *A three-dimensional finite-strain rod model. Part II: Computational aspects.* Computer Methods in Applied Mechanics and Engineering, 1986. 58(1): p. 79-116.
3. Cardona, A. and M. Geradin, *A beam finite element non linear theory with finite rotations.* International journal for numerical methods in engineering, 1988. 26(11): p. 2403-2438.
4. Hodges, D., *A mixed variational formulation based on exact intrinsic equations for dynamics of moving beams.* International Journal of Solids and Structures, 1990. 26(11): p. 1253-1273.
5. Hodges, D., *Geometrically exact, intrinsic theory for dynamics of curved and twisted anisotropic beams.* AIAA Journal 2003. 41(6): p. 1131-1137.
6. Cesnik, C. and D. Hodges, *VABS: A New Concept for Composite Rotor Blade Cross Sectional Modeling.* Journal of the American Helicopter Society, 1997. 42: p. 27.
7. Lee, C.-Y. and W. Yu, *Variational asymptotic modeling of composite beams with spanwise heterogeneity.* Journal of Computers and Structures, 2011. 89(15-16): p. 1503-1511.
8. Buannic, N. and P. Cartraud, *Higher-order effective modeling of periodic heterogeneous beams. I. Asymptotic expansion method.* International Journal of Solids and Structures, 2001. 38(40-41): p. 7139-7161.
9. Buannic, N. and P. Cartraud, *Higher-order effective modeling of periodic heterogeneous beams. II. Derivation of the proper boundary conditions for the interior asymptotic solution.* International Journal of Solids and Structures, 2001. 38(40-41): p. 7163-7180.
10. Kim, J.S. and K. Wang, *Vibration Analysis of Composite Beams With End Effects via the Formal Asymptotic Method.* Journal of Vibration and Acoustics, 2010. 132: p. 041003.
11. Kennedy, G.J. and J.R.R.A. Martins, *A homogenization-based theory for anisotropic beams with accurate through-section stress and strain prediction.* International Journal of Solids and Structures, 2012. 49(1): p. 54-72.
12. Ieşan, D., *On Saint-Venant's problem.* Archive for Rational Mechanics and Analysis, 1986. 91(4): p. 363-373.
13. Ieşan, D., *On the theory of uniformly loaded cylinders.* Journal of Elasticity, 1986. 16(4): p. 375-382.
14. Qiao, P. and L. Shan, *Explicit local buckling analysis and design of fiber–reinforced plastic composite structural shapes.* Composite Structures, 2005. 70(4): p. 468-483.
15. Geers, M.G.D., V. Kouznetsova, and W. Brekelmans, *Multi-scale computational homogenization: Trends and challenges.* Journal of Computational and Applied Mathematics, 2010. 234(7): p. 2175-2182.
16. Palacios, R., J. Murua, and R. Cook, *Structural and Aerodynamic Models in Nonlinear Flight Dynamics of Very Flexible Aircraft.* AIAA Journal, 2010. 48(11): p. 2648-2659.
17. Palacios, R. and C. Cesnik, *Cross-sectional analysis of nonhomogeneous anisotropic active slender structures.* AIAA journal, 2005. 43(12): p. 2624.
18. Cesnik, C.E.S. and M. Ortega-Morales, *Active composite beam cross-sectional modeling-stiffness and active force constants.* Proceedings of the 40th AIAA Structures, Structural Dynamics and Materials Conferences. St. Louis, Missouri, AIAA-99-1548, 1999.
19. Murua, J., et al., *Stability and Open-Loop Dynamics of Very Flexible Aircraft Including Free-Wake Effects*, in *52nd AIAA/ASME/ASCE/AHS/ASC Structures, Structural Dynamics and Materials Conference*2011: Denver, Colorado. p. 1-24.